Molecular Therapy
Original Article

The GPI-Linked Protein LY6A Drives AAV-PHP.B Transport across the Blood-Brain Barrier

Juliette Hordeaux,[1,4] Yuan Yuan,[1,4] Peter M. Clark,[1] Qiang Wang,[1] R. Alexander Martino,[1] Joshua J. Sims,[1] Peter Bell,[1] Angela Raymond,[2,3] William L. Stanford,[2,3] and James M. Wilson[1]

[1]Gene Therapy Program, Department of Medicine, University of Pennsylvania, Perelman School of Medicine, Philadelphia, PA 19104, USA; [2]Regenerative Medicine Program, Ottawa Hospital Research Institute, University of Ottawa, Ottawa, ON K1H 8L6, Canada; [3]Department of Cellular and Molecular Medicine, University of Ottawa, Ottawa, ON K1H 8L6, Canada

Efficient delivery of gene therapy vectors across the blood-brain barrier (BBB) is the holy grail of neurological disease therapies. A variant of the neurotropic vector adeno-associated virus (AAV) serotype 9, called AAV-PHP.B, was shown to very efficiently deliver transgenes across the BBB in C57BL/6J mice. Based on our recent observation that this phenotype is mouse strain dependent, we used whole-exome sequencing-based genetics to map this phenotype to a specific haplotype of lymphocyte antigen 6 complex, locus A (*Ly6a*) (stem cell antigen-1 [*Sca-1*]), which encodes a glycosylphosphatidylinositol (GPI)-anchored protein whose function had been thought to be limited to the biology of hematopoiesis. Additional biochemical and genetic studies definitively linked high BBB transport to the binding of AAV-PHP.B with LY6A (SCA-1). These studies identify, for the first time, a ligand for this GPI-anchored protein and suggest a role for it in BBB transport that could be hijacked by viruses in natural infections or by gene therapy vectors to treat neurological diseases.

INTRODUCTION

Gene therapy has successfully progressed into the clinic for the treatment of several rare monogenic diseases. A vector platform based on natural isolates of adeno-associated viruses (AAVs) has been essential to this success. We isolated and characterized a natural variant of AAV from human heart muscle called AAV9[1,2] that has shown superior distribution following intravenous (i.v.) delivery.[3–5] An AAV9-based vector approach to target motor neurons of patients with spinal muscular atrophy resulted in improved motor function and prolonged survival.[6] Similarly, impressive results have been achieved following i.v. delivery of an AAV8 serotype vector that we isolated from a macaque[7] in the treatment of children with a rare inherited myopathy (ClinicalTrials.gov: NCT03199469). Despite improvements in AAV vectors through the isolation of variants such as AAV8 and AAV9, most candidate diseases are outside the reach of successful *in vivo* gene therapy because of limited delivery to cells of target tissues.

An approach that we and others have pursued to improve the performance of AAV vectors is to engineer variants with enhanced efficiency. One strategy is to create diversity in capsid structure through population mutagenesis and select preferred candidates after iteratively screening the population in cells or animals. The most widely celebrated engineered AAV variant, called AAV-PHP.B, was shown by Deverman et al.[8] to have superior neurotropic properties. This research group created a library of variants by inserting randomized seven-amino-acid domains into the hypervariable region VIII of AAV9, and selected for those that target the CNS following i.v. injection into astrocyte-specific Cre recombinase-expressing mice in the C57BL/6J background. This selection process identified AAV-PHP.B, which contains a unique TLAVPFK peptide, and showed an amazing 50-fold improvement in CNS transduction following i.v. delivery into C57BL/6J mice.[8] This level of transduction would significantly expand the utility of AAV gene therapy for human neurological disorders. However, when we evaluated the use of AAV-PHP.B, we found a strain-specific effect in mice with widespread transduction of CNS cells achieved in C57BL/6J, but not BALB/cJ, mice.[9]

Through a combination of genetic and biochemical approaches, in this study we defined the factors allowing AAV-PHP.B to efficiently cross the blood-brain barrier (BBB) in a strain-specific manner. We determined that the high BBB permeability of AAV-PHP.B is based on the specific binding of the seven-amino-acid insert modified capsid to a glycosylphosphatidylinositol (GPI)-anchored protein expressed on brain endothelial cells called lymphocyte antigen 6 complex, locus A (LY6A, also known as stem cell antigen-1 [SCA-1]). Our findings suggest that in addition to its previously known roles in hematopoietic, mesenchymal, and cancer stem cell biology,[10–13] LY6A is involved in BBB transport.

RESULTS

BBB Permeability to AAV-PHP.B Is Inherited as a Codominant Trait in Mice

We previously showed that i.v. administration of 1×10^{12} genome copies (GCs) of AAV-PHP.B carrying the GFP transgene resulted

Received 24 January 2019; accepted 14 February 2019;
https://doi.org/10.1016/j.ymthe.2019.02.013.

[4]These authors contributed equally to this work.

Correspondence: James M. Wilson, MD, PhD, Gene Therapy Program, Department of Medicine, University of Pennsylvania, Perelman School of Medicine, 125 South 31st Street, Suite 1200, Philadelphia, PA 19104, USA.
E-mail: wilsonjm@upenn.edu

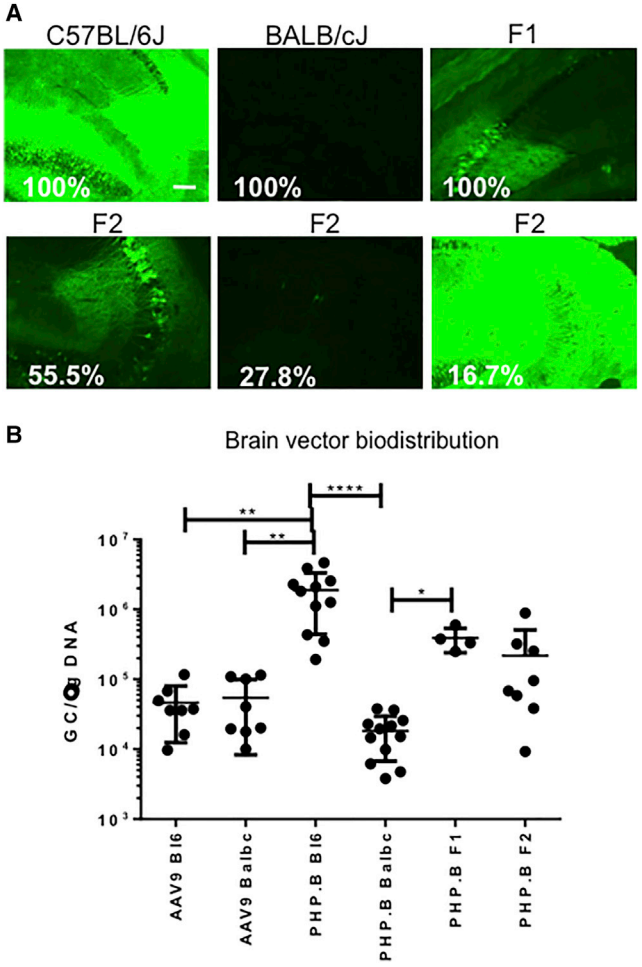

Figure 1. Permeability of the BBB to PHP.B Is Strain Specific and Inherited as a Codominant Trait in Mice

(A) Representative direct GFP fluorescence in the brain of inbred and intercrossed strains injected i.v. with 1×10^{12} GCs of AAV-PHP.B.CB7.EGFP. The percentage of F2 mice showing intermediate (55.5%), minimal (27.8%), and strong (16.7%) brain transduction is indicated on the corresponding images. A total of 18 F2 mice were injected. Scale bar, 100 µm. (B) Vector GCs measured by TaqMan qPCR in the brain, with averages per group and SDs as error bars. ANOVA Kruskal-Wallis test followed by Dunn's multiple comparison test: *p ≤ 0.05, **p ≤ 0.01, ****p ≤ 0.0001. See also Figure S1.

in widespread transduction of CNS cells in C57BL/6J mice, but not BALB/cJ, mice.[9] In contrast, direct administration of AAV-PHP.B into the CNS by intracerebroventricular injection, which bypasses the BBB, led to equally robust GFP expression in both C57BL/6J and BALB/cJ mouse brains close to the injection site; however, expression at a distance was more robust in C57BL/6J mice (Figure S1). Therefore, we concluded that in both mouse strains, CNS cells were susceptible to AAV-PHP.B brain transduction, but the higher efficiency of AAV-PHP.B in C57BL/6J mice was attributable to enhanced delivery across the BBB. We hypothesized that the strain-specific differences in permeability of the BBB to AAV-PHP.B was caused by a variation in a single gene involved in BBB transport. To test this hypothesis, we evaluated CNS transduction after i.v. administration of AAV-PHP.B in F1 and F2 progenies of C57BL/6J × BALB/cJ crossings. Whereas all F1 offsprings displayed intermediate CNS transduction compared with the parental strains, the F2 generation showed a distribution of transduction with 55.5% intermediate, 16.7% high C57BL/6J-like, and 27.8% low BALB/cJ-like CNS transduction (Figure 1A). We confirmed this result by using qPCR to quantify vector GC numbers in the corresponding mouse brains (Figure 1B). Based on phenotype distributions of F1 and F2, we conclude that BBB permeability to PHP.B follows the Mendelian inheritance pattern of two codominant alleles at a single genomic locus. In contrast with AAV-PHP.B, we did not observe any strain-specific brain transduction for AAV9 (Figure 1B).

Ly6a Is Linked to PHP.B Transduction across the BBB

The CNS transduction inheritance pattern in F1 and F2 progenies suggests that variations in a single gene underlie the strain-specific differences in this phenotype (i.e., high BBB permeability to AAV-PHP.B). We therefore conducted a whole-exome sequencing (WES)-based genotyping and genetic linkage analysis of 16 related mice to identify potential causal mutations within and around exonic regions of the mouse genome (Figure 2A). We identified 135 unique mutations within a ~4.5-Mbp stretch of genomic DNA spanning the D3 and E3 karyotype bands of murine chromosome 15 that were most significantly associated ($p = 1.9E{-}31$) with the observed phenotype (Figure 2B). Functional variant annotation of the significant variants ($p \leq 5E{-}8$) revealed that missense mutations within the *Ly6a*, *Ly6i*, *Rhophilin 1*, and *Riken* cDNA 2010109I03 genes were most significantly linked with low BBB permeability to AAV-PHP.B (Table S1). Based on the subcellular localization of the proteins encoded by these genes and their abundance in the brain according to public databases,[14] we hypothesized that the causative protein was LY6A, a GPI-anchored surface protein also known as SCA-1 that is highly expressed in the brain microvasculature. To test whether *Ly6a* is essential for the efficient delivery of AAV-PHP.B across the BBB, we i.v. injected AAV-PHP.B carrying the GFP transgene in *Ly6a* knockout mice ($Ly6a^{-/-}$) in the C57BL/6J background and wild-type (WT) controls. Although AAV-PHP.B transduced liver in both WT and $Ly6a^{-/-}$ mice, we observed minimal brain transduction in $Ly6a^{-/-}$ mice (Figure 2C). This indicates that LY6A is required for AAV-PHP.B transport across the BBB. Interestingly, polymorphisms in the *Ly6* gene cluster have been described previously,[15] with two major haplotypes in inbred strains: $Ly6^a$ (BALB/cJ-like) and $Ly6^b$ (C57BL/6J-like). These two haplotypes differ with respect to several single-nucleotide changes within the promotor region and two amino acid substitutions in the LY6A protein (i.e., the $Ly6^a$-encoded proteins have Val106Ala and pAsp63Gly substitutions relative to $Ly6^b$). Upon analyzing the brain tissue via immunohistochemistry with a pan-LY6A antibody, we observed a high level of expression in the microvascular endothelial cells of C57BL/6J animals. In contrast, LY6A expression was substantially reduced in BALB/cJ animals (Figure 2D), consistent with previous reports.[16] We detected no expression of LY6A in tissue from $Ly6a^{-/-}$ mice, thus confirming the specificity

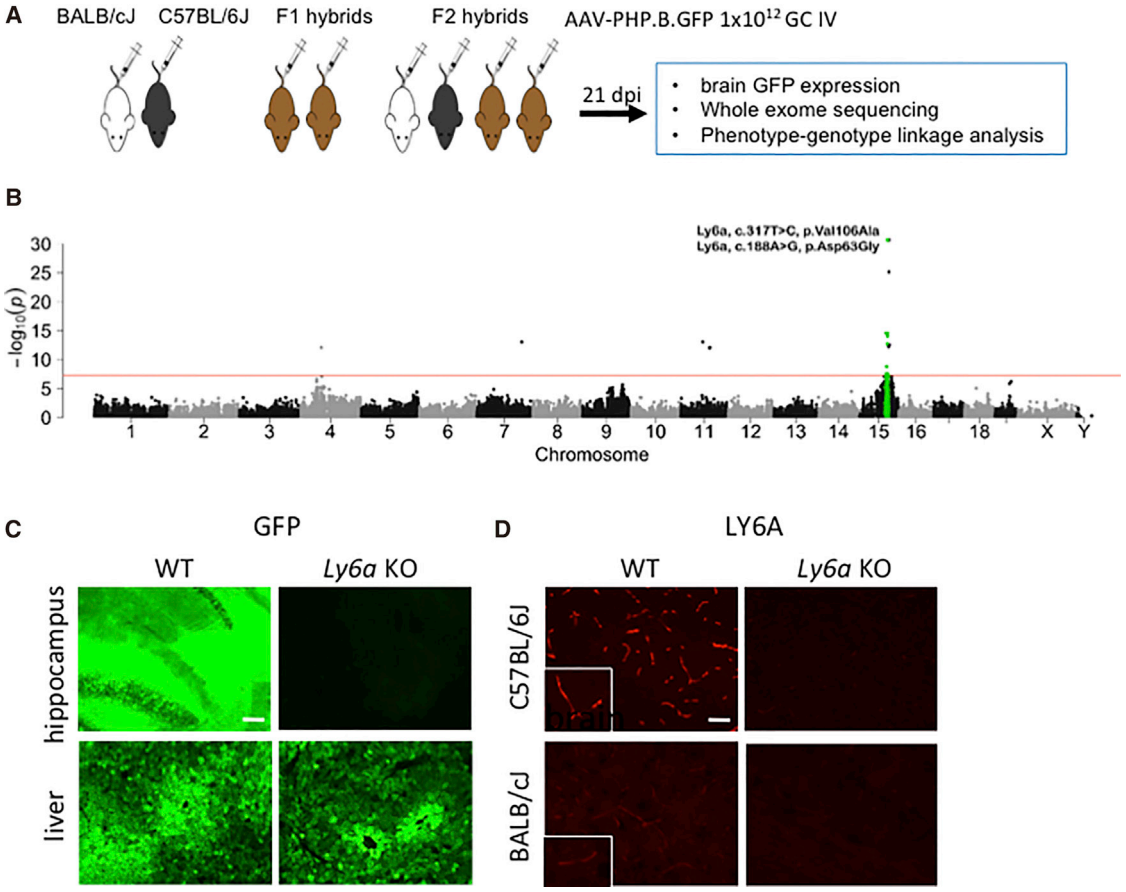

Figure 2. The *Ly6a* Gene Is Associated with High AAV-PHP.B Transduction across the BBB

(A) WES association study design overview. We generated F1 hybrids by crossing the inbred strains C57BL/6J and BALB/cJ, producing heterozygotes with an intermediate brain transduction phenotype. F2 hybrids were generated by intercrossing F1 mice, producing a variety of phenotypes and genotypes. WES was performed on genomic DNA isolated from the brains of 16 mice (4 F1 and 12 F2), and reads were mapped to the reference genome (GRCm38, C57BL/6J). (B) Manhattan plot, showing genetic variants that are significantly associated (red line, $p \leq 5E{-}8$) with PHP.B transduction across the BBB in mice. We observed the strongest association within the D3 karyotype band (colored in green), which includes the two labeled missense mutations within the *Ly6a* gene. (C) Genetic confirmation that the presence of *Ly6a* is necessary for AAV-PHP.B brain transduction across the BBB *in vivo*. Representative images show direct GFP fluorescence in the hippocampus (top) and liver (bottom) of inbred WT and *Ly6a* null mice in the C57BL/6J background after i.v. administration of 1×10^{12} GCs of AAV-PHP.B.CB7.EGFP. (D) LY6A immunostaining in the cerebral cortex of knockout (KO) and WT mice using an antibody that recognizes both haplotypes (clone D7). LY6A expression was mainly confined to the brain capillaries and was high in C57BL/6J WT mice, weak in BALB/cJ WT mice, and undetectable in all KO mice. Scale bars, (C) 100 μm and (D) 50 μm.

of the assay (Figure 2D). Either the promoter mutations or those within the open reading frame of BALB/cJ LY6A could contribute to the drastically decreased LY6A expression on brain endothelium. In agreement with our findings, a study reported an approximately 4-fold decrease in *Ly6a* mRNA levels in the CNS of $Ly6^a$ compared with $Ly6^b$ mouse strains (RNA-sequencing data).[17]

Based on these observations, we hypothesized that the strain-specific BBB permeability of AAV-PHP.B observed in C57BL/6J and BALB/cJ mice could be generalized across all strains of mice with $Ly6^b$ and $Ly6^a$ haplotypes. To test this hypothesis, we obtained six additional inbred strains of mice, three with the $Ly6^b$ haplotype (129S1/Svlmj, DBA2/J, and FVB/NJ) and three with the $Ly6^a$ haplotype (C3H/HeJ, CBA/J, and A/J; see Figure 3A). We i.v. infused mice from each strain with AAV-PHP.B expressing GFP and subsequently analyzed them for CNS transduction. As predicted, high levels of CNS transduction directly correlated with the $Ly6^b$ (C57BL/6J-like) haplotype (Figure 3B). Taken together, we conclude that *Ly6a* gene variants are linked to PHP.B transduction across the BBB.

AAV-PHP.B and AAV-PHP.eB Bind to LY6A Protein with High Affinity

We developed ELISAs to evaluate the potential for direct interactions between LY6A and AAV capsids. We constructed expression cassettes containing a GPI-anchor truncated version of the C57BL/6J LY6A to isolate the soluble version of the recombinant protein. We performed an ELISA assay by analyzing the binding of AAV particles to the recombinant LY6A protein bound to the ELISA

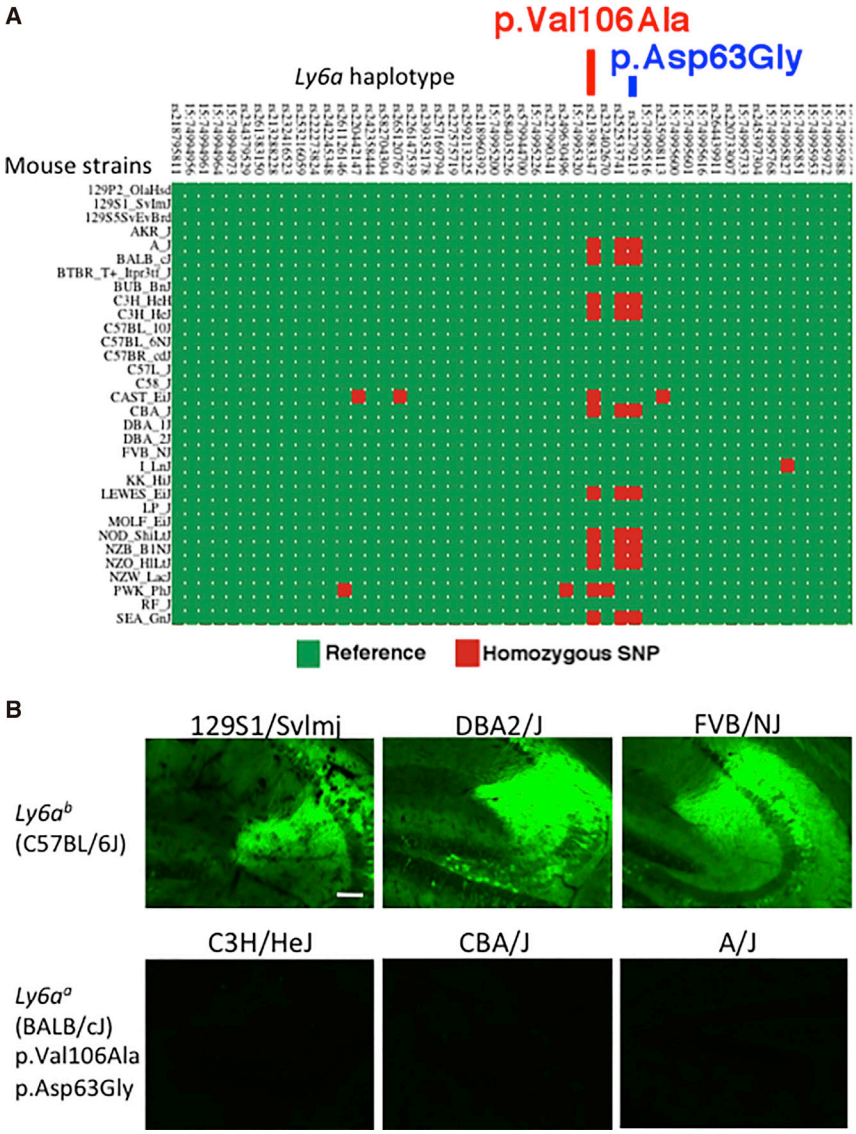

Figure 3. *Ly6a* Haplotype Determines the Ability of AAV-PHP.B to Cross the BBB in Mice

(A) *Ly6a* haplotypes from a selection of inbred mice (data compiled from the mouse genome project, MM10 dbSNP142). (B) AAV-PHP.B brain transduction after systemic administration in inbred mice with the reference *Ly6a* gene ($Ly6^b$ haplotype, C57BL/6J-like) and strains with the BALB/cJ-like SNP ($Ly6^a$ haplotype). Scale bar, 100 μm.

well (Figure 4A). AAV-PHP.B bound LY6A with high apparent affinity, with ELISA data closely fitting a subnanomolar isotherm (0.07 nM). We suspect this high affinity represents the avid engagement of multiple immobilized LY6A proteins with AAV-PHP.B vectors. We did not detect any binding between AAV9 and the LY6A protein (Figure 4A). Next, we generated a variant capsid AAV-PHP.B V592G with a single-amino-acid mutation in the seven-amino-acid loop of AAV-PHP.B (i.e., valine to glycine on VP1 position 592 in the fourth residue of the seven-amino-acid insert). The expression profile following i.v. injection of a GFP-expressing version of this mutant capsid resembled that of AAV9, but not AAV-PHP.B: high liver but little CNS transduction (Figure S2). Interestingly, neither AAV9 nor AAV-PHP.B V592G bound detectibly to LY6A (Figure 4A), showing a direct link between capsid interaction with LY6A *in vitro* and the ability to cross the BBB in *vivo*, which supports a role for LY6A as a receptor or co-receptor for AAV-PHP.B.

We then studied the ability of LY6A to enhance the internalization of AAV capsids. In this assay, we transiently transfected the full-length C57BL/6J *Ly6a* coding sequence into HEK293 cells that were subsequently incubated with AAV-PHP.B or AAV9 expressing lacZ. In this assay, we used transgene (LacZ) expression, measured by β-galactosidase activity in cell lysates, as a proxy for internalization. Transduction was achieved in a dose-dependent manner with AAV-PHP.B incubated with cells expressing the LY6A protein (Figure 4B). There was no transduction over background with AAV9 on cells that expressed LY6A or with AAV-PHP.B on cells that expressed the related GPI-anchored protein LY6C1 (Figure 4B). Moreover, we could prevent the LY6A-enhanced transduction of AAV-PHP.B by pre-incubating cells with an anti-LY6A rat monoclonal antibody, but not an isotype control (Figure 4C). This result lends further support to the hypothesis of a co-receptor or receptor role for LY6A.

A recent study described a second-generation version of AAV-PHP.B, called AAV-PHP.eB, with an even higher transduction of CNS in C57BL/6J mice following i.v. injection. We studied this variant to determine whether LY6A remained the primary determinant of BBB permeability. Following i.v. injection of AAV-PHP.eB, we observed CNS transduction in C57BL/6J mice, but not BALB/cJ mice, similar to our observations with AAV-PHP.B (Figure S3). AAV-PHP.eB bound to C57BL/6J LY6A with subnanomolar apparent affinity and a slightly higher maximum signal than that achieved with AAV-PHP.B (Figure 4A). We conclude that interactions with LY6A remain critical to the neurotropic properties of both AAV-PHP.B and AAV-PHP.eB.

DISCUSSION

As the technology of gene transfer has progressed, so has our understanding of key performance drivers like transduction efficiency and host-vector responses. Some of these translational studies have

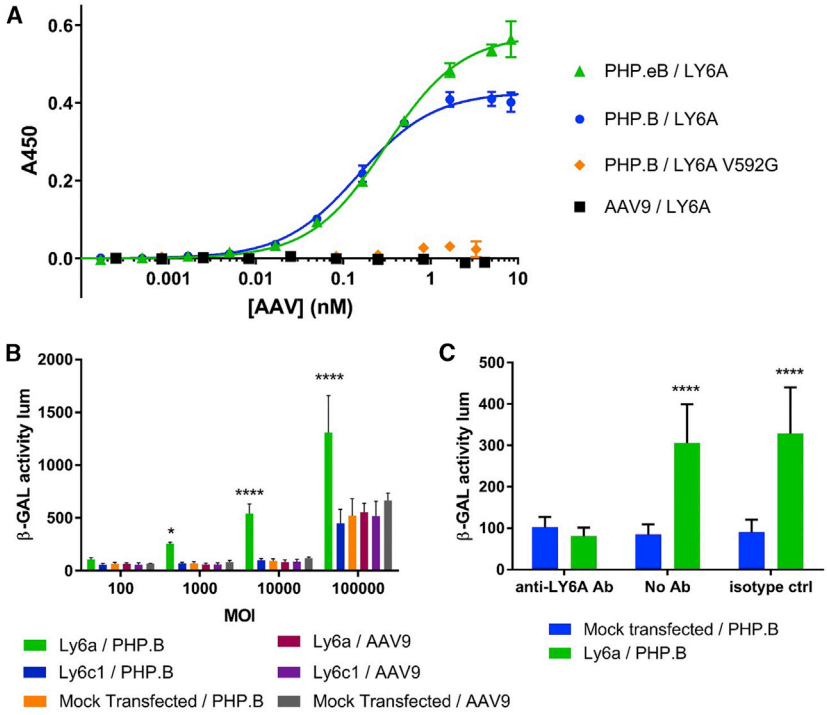

Figure 4. AAV-PHP.B Binds to LY6A Proteins

(A) ELISA measurement of the binding of AAV-PHP.B, AAV-PHP.eB, AAV9, or an inactive AAV-PHP.B V592G mutant to the C57BL/6J LY6A protein. Data points represent the average of three replicates with error bars denoting the SEM. (B) AAV.LacZ transduction assay in *Ly6a*-transfected cells. HEK293 cells were transiently transfected with LY6A- or LY6C1-expressing vectors, followed by incubation with AAV variants carrying the LacZ transgene. Twenty-four hours later, AAV transduction was evaluated by LacZ expression. Transient expression of C57BL/6J *Ly6a* in HEK293 cells enhanced AAV-PHP.B, but not AAV9, transduction, whereas another *ly6* family member, *ly6c1*, had no effect. AAV9- and AAV-PHP.B-mediated transduction efficiency within the same transfection conditions were compared using two-way ANOVA followed by a mean comparison test using Tukey's multiple comparison test (GraphPad Prism); *$p \leq 0.05$, ****$p \leq 0.0001$. (C) AAV.-LacZ transduction assay in the presence of anti-LY6A antibody. Enhanced AAV-PHP.B transduction (MOI of 10,000) was prevented by preincubating transfected cells with an anti-LY6A antibody (clone D7, 100 nM, 1 h at 4°C). Transduction efficiencies in the presence of different antibodies were compared within the same transfection conditions using two-way ANOVA followed by a mean comparison test using Tukey's multiple comparison test (GraphPad Prism); ****$p \leq 0.0001$. The bar graphs show the average of (B) six or (C) eight replicates, with error bars representing SD. See also Figures S2 and S3.

enhanced our understanding of related fundamental biological processes. The ability of AAV vectors to transduce cells in the CNS of all mammals in a deliberate and dose-dependent manner has revolutionized the field of neurobiology through the advent of tools such as optogenetics (reviewed in Betley and Sternson[18]). In studies designed to blunt adaptive immune responses to *in vivo* gene transfer with adenoviruses, we have discovered the mechanism by which CD40 engages with CD40 ligand (CD40L) to activate T cells.[19] The story described in this paper is another example of translational work illuminating a new biological principle that has impacts beyond gene therapy.

The AAV9 variant AAV.PHP.B was heralded as potentially transforming the treatment of neurological diseases. The efficiency with which it could transduce CNS cells after i.v. injection in C57BL/6J mice was at least 50-fold higher than what had been previously achieved. If translated to primates, AAV.PHP.B would enable the development of treatments across a broad array of neurological diseases.[20] Our initial evaluation of AAV-PHP.B led to the serendipitous discovery that its BBB permeability was limited to some strains of mice such as C57BL/6J.[9] The substantial difference in transduction biology between two related, but genetically distinct, strains of mice such as C57BL/6J and BALB/cJ allowed us to use a classic genetic linkage approach to show that a single gene determines this dramatic strain difference in BBB permeability and that this gene encodes the GPI-anchored protein LY6A.

LY6A, also called SCA-1, was discovered more than 40 years ago as an antigen that is upregulated on activated lymphocytes. It is commonly used to enrich adult murine hematopoietic stem cells (HSCs) and is also expressed on stem cells, progenitors, and differentiated cell types across a wide variety of tissues and organs (reviewed in Holmes and Stanford[10]). It is fascinating that despite its common use in stem cell biology research, ligand(s) of LY6A have not yet been identified.[21–23] Although its physiological functions are also unclear, studies of *Ly6a* null mice suggest a role in downregulating T cell proliferation;[24] regulating hematopoiesis lineage, engraftment, and homing of HSCs;[11,25] promoting the self-renewal of mesenchymal stem cells; and regulating bone formation.[26,27] In the present study, we made the novel discovery of a ligand for LY6A (i.e., the AAV9 capsid variant AAV.PHP.B), and we demonstrated a direct link between the binding of this ligand to LY6A and its ability to cross the BBB. LY6A is highly expressed in brain microvasculature,[14,16,28] and the $Ly6^b$ haplotype was previously linked to WT mouse adenovirus 1-induced lethal encephalitis.[29,30] In this context, our results suggest that this murine GPI-anchored protein could play a role in viral interaction and transcytosis at the BBB.

Studies of other GPI-anchored proteins suggest various mechanisms by which LY6A could enhance BBB permeability of AAV vectors. GPI-anchored proteins are localized to lipid rafts, which are dynamic microdomains within the plasma membrane that are enriched in cholesterol, sphingolipids, and a specific set of key signaling molecules such as receptors and protein tyrosine kinases. The apical-to-basolateral delivery of raft-associated GPI-anchored proteins occurs via a transcytotic pathway in polarized cells.[31] Furthermore, transcytosis of macromolecules at the BBB can occur, in part, via tightly regulated caveolae-associated lipid rafts.[32] Some GPI-anchored proteins, and

lipid rafts in general, play a role in the cell entry and exit of virus particles (reviewed in Metzner et al.[33]). Interestingly, group B coxsackieviruses cross epithelial barriers through a three-step mechanism involving: (1) interaction with the apically localized GPI-anchored protein CD55 (aka, decay-accelerating factor); (2) CD55 clustering and activation of AbI kinase driving Rac-dependent actin reorganization; and (3) translocation of viral particles to lateral tight junctions where the particles engage their receptor, the coxsackievirus-adenovirus receptor, and undergo endocytosis.[34] In this model, GPI-anchored proteins allow for the initial capture of viral particles and trigger transport of the virus to a receptor buried in the tight-junction area. In the case of AAV-PHP.B transduction across the BBB, further experiments are necessary to determine whether LY6A is a co-receptor that facilitates the co-localization of viral capsids with other factors, or if LY6A acts as the main receptor through cross-linking activated endocytosis.

Experimental data suggest that AAV9 crosses the BBB without compromising its integrity via transendothelial trafficking to the basolateral compartment.[35] The efficiency with which this occurs, however, is at least 20-fold lower than what is achieved with AAV-PHP.B in C57BL/6J mice.[8] Other AAV serotypes such as AAV5 can cross epithelial and endothelial barriers *in vitro* through transcytosis, a phenomenon that can be blocked by tannic acid or filipin,[36] two chemicals that interfere with GPI-anchored protein-mediated transport. Interestingly, some researchers have suggested that the major transduction route that recombinant AAV2 uses is the CLathrin-Independent Carriers GPI-anchored-protein-Enriched Endosomal Compartment.[37] Those studies, conducted by independent groups, combined with the work reported here collectively support a central role of GPI-enriched lipid rafts in AAV transcytosis and/or transduction. Our group is the first to show that a particular GPI-anchored protein acts as a co-receptor or receptor for AAV vectors.

Our study suggests that GPI-anchored proteins could be hijacked to improve the delivery of biotherapeutics to the brain. However, several groups including ours have failed to demonstrate increased CNS transduction following i.v. injection of AAV-PHP.B in non-human primates.[9,38] This failure can be explained by the absence of a LY6A homolog in primates.[39] In fact, the only animal models that show enhanced BBB permeability of AAV.PHP.B are those with genetic backgrounds similar to the model in which it was selected (i.e., C57BL/6J mice). This fact illustrates how the method of selecting novel capsid variants can limit the utility of candidate capsids. When developing human gene therapy vectors and other protein therapeutics, it may be more productive to evaluate populations of variants for binding to GPI-anchored proteins expressed on endothelial cells derived from primates.

MATERIALS AND METHODS

Contact for Reagent and Resource Sharing

Further information and requests for resources and reagents should be directed to and will be fulfilled by the lead contact, James M. Wilson (wilsonjm@upenn.edu).

Experimental Model and Subject Details

Animals

C56BL/6J (stock no. 000664), BALB/cJ (000651), F1 hybrids CB6F1/J (100007), 129S1/SvlmJ (002448), DBA/2J (000671), FVB/NJ (001800), C3H/HeJ (000659), CBA/J (000656), and A/J (000646) mice were purchased from the Jackson Laboratory. F2 hybrids were obtained by crossing CB6F1/J at the facility. *Ly6a* null mice on a C57BL/6J and BALB/cJ background were generously provided by William L. Stanford (University of Ottawa). For reporter gene experiments, adult (6–8 weeks old) males were injected. Animals were housed in standard caging of two to five animals per cage. Cages, water bottles, and bedding substrates were autoclaved in the barrier facility, and cages were changed once per week. An automatically controlled 12-h light or dark cycle was maintained. Each dark period began at 7:00 p.m. (±30 min). Irradiated laboratory rodent food was provided *ad libitum*.

Cell Lines

HEK293 (originally obtained from a female embryo) cells were maintained in DMEM (catalog no. [Cat#] 11995-040; GIBCO, Thermo Fisher Scientific, Waltham, MA, USA) supplemented with gamma-irradiated 10% fetal bovine serum (Cat# SH30071.03IR; Hyclone; GE Healthcare, Pittsburgh, PA, USA) and 100 IU/mL penicillin and streptomycin (P/S), and grown in a humidified incubator at 37°C with 5% CO_2.

Method Details

Vector Production

The AAV9.PHP.B *trans* plasmid (pAAV2/PHP.B) was generated with a QuikChange Lightning Site-Directed Mutagenesis Kit (Cat# 210515; Agilent Technologies, Santa Clara, CA, USA) using pAAV2/9 (Penn Vector Core) as the template, following the manufacturer's manual. The AAV-PHP.B mutants were constructed the same way using pAAV2/PHP.B as the template. AAV vectors were produced and titrated by the Penn Vector Core as described before.[40] In brief, HEK293 cells were triple transfected, and the culture supernatant was harvested, concentrated, and purified with an iodixanol gradient. The purified vectors were titrated with droplet digital PCR using primers targeting the rabbit Beta-globin polyA sequence as previously described.[41]

In Vivo *Studies and Histology*

Mice received 1×10^{12} GCs (5×10^{13} GC/kg) of AAV9, AAV-PHP.B, or AAV-PHP.eB vectors encoding EGFP (Penn Vector Core) in 0.1 mL via the lateral tail vein and were euthanized by inhalation of CO_2 21 days post-injection. Tissues were promptly collected, starting with brain. Half sagittally sectioned brain was immersion fixed in 10% neutral-buffered formalin for about 24 h, washed briefly in PBS, and equilibrated sequentially in 15% and 30% sucrose in PBS at 4°C. Tissues were then frozen in optimum cutting temperature embedding medium and cryosectioned for direct GFP visualization (brains were sectioned at 30 μm, other tissues at 10 μm thickness). Images were either acquired with a Nikon Eclipse Ti-E fluorescence microscope or whole-brain sections were scanned with an Aperio Versa slide

scanner. The other half of the brain was either snap-frozen on dry ice for the qPCR vector biodistribution study, or formalin-fixed and paraffin-embedded for immunostaining. Immunofluorescence for LY6A was performed on formalin-fixed, paraffin-embedded brain samples. Sections were deparaffinized, boiled for 6 min in 10 mM citrate buffer (pH 6.0) for antigen retrieval, blocked with 1% donkey serum in PBS + 0.2% Triton for 15 min, and then sequentially incubated with primary (1 h) and fluorescence-labeled secondary antibodies (45 min) diluted in blocking buffer. Monoclonal rat antibody D7 against LY6A (Cat# 14-5981-82; eBioscience, Thermo Fisher Scientific, San Diego, CA, USA) was used at a dilution of 1:200, and tetramethylrhodamine (TRITC)-labeled donkey anti-rat (Cat# 712-025-153; 1:100 dilution; Jackson Immunoresearch, West Grove, PA, USA) was served as secondary antibody.

Vector Biodistribution

Tissue DNA was extracted with a QIAamp DNA Mini Kit (Cat# 51306; QIAGEN, Germany), and vector genomes were quantified by real-time PCR using TaqMan reagents (Applied Biosystems, Life Technologies, Foster City, CA, USA) and primers and probes targeting the rabbit beta-globin (rBG) polyadenylation sequence of the vectors.

Whole-Exome Sequencing

WES libraries were generated from genomic DNA isolated from the brains of 4 F1 and 12 F2 mice using the Agilent SureSelect Mouse All Exon Kit (Cat 5190-4641; Agilent). Samples were indexed and sequenced on a NextSeq high-output cartridge (eight samples per flow cell). Following sequencing, paired-end reads from each sample were mapped to the reference genome (GRCm38) using NovoAlign (v3.08.02) with optimized parameters for WES.[42] Duplicate reads (optical and/or PCR duplicates that originate from a single fragment of DNA) were subsequently flagged with Picard tools (v2.13.2). Following data pre-processing, variant calling was performed for each sample using Genome Analysis Tool Kit (GATK) best practices.[43–46] In brief, base quality score recalibration was performed first, followed by variant calling and joint genotyping using GATK (v3.8). Raw variants were subsequently filtered to remove Mendelian violations and variants with a quality score of 50 or less. High-confidence variants were subsequently used for association testing (see Statistics). Genomic variant annotation and functional effect prediction were performed using SnpEff.[47]

Ly6a Expression Vector Construction

LY6A coding sequence from C57BL/6J was synthesized as a GeneArt String (Thermo Fisher Scientific). For native LY6A expression vectors, GeneArt String was assembled into BamHI-digested pcDNA3.1(+)IRES GFP (plasmid 51406; Addgene, Cambridge, MA, USA) using the NEBuilder HiFi DNA Assembly Master Mix (Cat# E2621; NEB, Ipswich, MA, USA). For the Twin-Strep-tagged LY6A expression vectors, DNA encoding the first 111 amino acid residues of LY6A was PCR amplified before assembly into Esp3I-digested pESG-IBA103 using the NEBuilder HiFi DNA Assembly Master Mix (Cat# E2621; NEB). All constructs were confirmed by Sanger sequencing.

Twin-Strep-Tagged LY6A Production and Purification

HEK293 cells were transiently transfected with plasmids expressing Twin-Strep-tagged C57BL/6J LY6A using a 1:2 DNA-to-polyethylenimine (PEI; linear PEI hydrochloride molecular weight [MW] 40,000; Cat# 24765-1; Polysciences, Warrington, PA, USA) w/w ratio. Seventy-two hours post-transfection, cell culture supernatants were filtered through 0.22-μm filters and adjusted to pH 8.0 by adding one-tenth volumes of 10× Buffer W (1 M Tris-HCl [pH 8.0], 1.5 M NaCl, 10 mM EDTA). Transfected HEK293 cells were lysed in 1× Buffer W supplemented with 0.1% Triton X-100 and passaged twice through 27G needles. Cell lysates and culture supernatants were combined followed by biotin depletion through a 15-min incubation with 1/400 volume of BioLock Biotin Blocking Solution (Cat# 2-0205-050; IBA Life Sciences) and subsequent centrifugation. Purification of Twin-Strep-tagged LY6A protein was achieved through Strep-Tactin XT affinity chromatography according to the manufacturer's protocol (IBA Life Sciences). In brief, Strep-Tactin XT Superflow resin (Cat# 2-4010-010; IBA Life Sciences, Germany) was incubated with cell lysates and supernatant for 2 h at room temperature, washed with four column volumes (CVs) of 1× Buffer W, and eluted with 0.6, 1.6, and 0.8 CV of 1× Buffer BXT. Eluate fractions containing recombinant LY6A were pooled and dialyzed four times in 50 mM Tris-HCl (pH 8.0), 150 mM NaCl. Protein concentrations were determined by bicinchoninic acid assay (Cat# 23225; Pierce, Rockford, IL, USA).

ELISA

Strep-Tactin XT-coated microplates (Cat# 2-4101-001; IBA Life Sciences) were incubated overnight at 4°C with 200 μL of coating buffer (50 mM Tris-HCl [pH 8.0], 150 mM NaCl) containing 0 or 0.5 μg of Twin-Strep-tagged LY6A proteins per well. Plates were washed 3× with PBST (0.05% Tween 20 in PBS) and blocked in 3% BSA in PBS for 2 h at room temperature. AAV serotypes were diluted in PBS supplemented with 1% BSA and 0.1% Pluronic F-68 to the indicated concentrations. We added 200 μL of AAV dilutions to each well and incubated them for 2 h at 37°C. Immobilized AAV particles were detected by sequential 1-h incubations with a rabbit antiserum against AAV9 (1:50,000; Penn Immunology Core) and a horseradish peroxidase-conjugated goat anti-rabbit secondary antibody (1:5,000, Cat# 31460; Thermo Fisher Scientific). We developed plates using 200 μL of the SureBlue TMB 1-component microwell Peroxidase Substrate (Cat# 52-00-01; Seracare, Gaithersburg, MD, USA) per product instructions, and optical densities were measured at 450 nm by a microplate reader (SpectraMax M3). To calculate LY6A-dependent AAV binding, background AAV bindings to uncoated microplate wells were subtracted from the observed AAV bindings to LY6A-coated wells at each virus concentration. Data are representative of three independent experiments. To estimate the apparent affinity (K_d) of AAV-PHP.B variants for LY6A, we applied least-squares fitting of the ELISA data (A450 signal as a fraction of the maximum) to a simple 1:1 model for molecular interaction

[$f = At/(K_d + At)$], where f is the fraction of LY6A bound, and At is the total amount of AAV applied to the well. A more complex model that accounted for LY6A explicitly did not improve the fit. The ELISA orientation used allows us only to estimate the apparent affinity of a vector for a field of LY6A protein, as might be encountered on a cell, and does not represent the microscopic affinity of a single PHP.B peptide loop with a single LY6A protein.

HEK293 Transduction Assay

All cell culture was performed in a humidified incubator at 37°C + 5% CO_2 using DMEM (10-013-CM; Corning) + 10% heat-inactivated fetal bovine serum (10438-034; GIBCO) + 1% P/S (15140-122; GIBCO). On the first day of the assay, HEK293 cells were trypsinized, counted, and seeded on 96-well plates (Cat# 3603; Corning Life Sciences, Corning, NY, USA) at a density of 80,000 cells/well. After 24 h, plasmid constructs containing the C57BL/6J Ly6a or Ly6c1, upstream of an IRES2-EGFP sequence, were transiently transfected into cells. Transfection was performed in serum-free DMEM using 0.28 μg of plasmid DNA and 0.56 μg of PEI per well in a culture volume of 100 μL. Mock-transfected cells received only PEI in serum-free DMEM. Twenty-four hours post-transfection, each well was supplemented with 100 μL DMEM + 20% FBS + 1% P/S and allowed to expand under full-serum conditions for an additional 24 h. After 24 h, GFP expression was assessed qualitatively in transfected wells using a fluorescence microscope. AAV9 and AAV9-PHP.B viral vectors containing a beta-galactosidase reporter gene under control of a CMV promoter were then introduced to each well at an MOI ranging from 100,000 to 10. This transduction step was performed in 100 μL of serum-free DMEM for 2 h, followed by addition of 100 μL DMEM + 20% FBS + 1% P/S and incubation for 24 h. Beta-galactosidase expression was then determined using the Galacto-Star B-Galactosidase Reporter Gene Assay System (T1014; Thermo Fisher Scientific) as per the manufacturer's Direct Lysis Protocol for Microplate Cultures. The lysis step of this protocol was modified in that 40 μL of lysis buffer was used per well, and lysis was performed for 30 min. Luminescence detection was then performed on a SpectramaxM3 Luminescence Plate Reader. Data are representative of six independent experiments.

HEK293 Antibody Inhibition Assay

The HEK293 Antibody Inhibition Assay was performed as described above in the HEK293 Transduction Assay with the following modifications or additions. Only the Ly6a-IRES2-EGFP plasmids were used in transfection. Additionally, an antibody incubation step was added before AAV9-PHP.B transduction on day 4 of the assay. In this step, D7 endotoxin-low and azide-free anti-LY6A antibody (Cat# 31-2027; Abeomics, San Diego, CA, USA) or IgG isotype control (Cat# 18450; Abcam, Cambridge, MA, USA) was incubated with cells for 1 h at 4°C. Antibodies were introduced in 50 μL of serum-free DMEM at 100 nM and following this incubation, AAV9-PHP.B reporter vector was introduced in 50 μL of serum-free DMEM at an MOI of 10,000. Plates were then returned to the 37°C incubator, and the remainder of the assay proceeded as previously described. Data are representative of eight independent experiments.

Statistics

Vector GCs in mice were analyzed using a one-way ANOVA (Kruskal-Wallis test) followed by Dunn's multiple comparisons test with an alpha value of 0.05 (GraphPad Prism). For WES linkage analysis, trait-associated variants were identified using a linear Wald test for quantitative traits (https://github.com/statgen/EPACTS). Only variants with a p value $\leq 5E{-}8$ were considered significant. HEK293 transduction efficiencies (beta-galactosidase activity) were compared using a two-way ANOVA followed by a mean comparison test using Tukey's multiple comparison test (GraphPad Prism).

Study Approval

All animal protocols were approved by the Institutional Animal Care and Use Committee of the University of Pennsylvania, and animals were housed in an Association for Assessment and Accreditation of Laboratory Animal Care International-accredited barrier facility within the School of Medicine at the University of Pennsylvania. The University of Pennsylvania's Office of Laboratory Animal Welfare Assurance Number is A3079-01.

SUPPLEMENTAL INFORMATION

Supplemental Information includes three figures and one table and can be found with this article online at https://doi.org/10.1016/j.ymthe.2019.02.013.

AUTHOR CONTRIBUTIONS

Conceptualization: J.H. and J.M.W.; Methodology: J.H., Y.Y., P.M.C., Q.W., and P.B.; Software: P.M.C.; Formal Analysis: P.M.C. and J.J.S.; Investigation: J.H., Y.Y., P.M.C., Q.W., R.A.M., and A.R.; Resources: W.L.S.; Writing – Original Draft: J.H., Y.Y., P.M.C., and J.J.S.; Writing – Review & Editing: J.H. and J.M.W.; Supervision: J.H. and J.M.W.; Funding Acquisition: J.M.W.

CONFLICTS OF INTEREST

J.M.W. is an advisor to, holds equity in, and has a sponsored research agreement with Scout Bio and Passage Bio; he also has a sponsored research agreement with Ultragenyx, Biogen, Janssen, Precision Biosciences, Moderna Therapeutics, and Amicus Therapeutics, which are licensees of Penn technology. J.M.W. holds equity in REGENXBIO; he is also an inventor on patents that have been licensed to various biopharmaceutical companies. J.M.W., J.H., and J.S.S. are inventors on patent applications related to AAV vectors and AAV gene therapy.

ACKNOWLEDGMENTS

We would like to acknowledge the University of Pennsylvania Gene Therapy Program cores: Penn Vector Core, Morphology Core, Biostatistics and Bioinformatics Core, Nucleic Acid Technologies Core, and Program for Comparative Medicine. We also thank Liying Han, Tahsin Jahan, Brianne Jeffrey, and Laura Ballentine for invaluable technical assistance.

REFERENCES

1. Gao, G., Vandenberghe, L.H., Alvira, M.R., Lu, Y., Calcedo, R., Zhou, X., and Wilson, J.M. (2004). Clades of Adeno-associated viruses are widely disseminated in human tissues. J. Virol. *78*, 6381–6388.
2. Bell, C.L., Vandenberghe, L.H., Bell, P., Limberis, M.P., Gao, G.P., Van Vliet, K., Agbandje-McKenna, M., and Wilson, J.M. (2011). The AAV9 receptor and its modification to improve in vivo lung gene transfer in mice. J. Clin. Invest. *121*, 2427–2435.
3. Zincarelli, C., Soltys, S., Rengo, G., and Rabinowitz, J.E. (2008). Analysis of AAV serotypes 1-9 mediated gene expression and tropism in mice after systemic injection. Mol. Ther. *16*, 1073–1080.
4. Duque, S., Joussemet, B., Riviere, C., Marais, T., Dubreil, L., Douar, A.M., Fyfe, J., Moullier, P., Colle, M.A., and Barkats, M. (2009). Intravenous administration of self-complementary AAV9 enables transgene delivery to adult motor neurons. Mol. Ther. *17*, 1187–1196.
5. Bevan, A.K., Duque, S., Foust, K.D., Morales, P.R., Braun, L., Schmelzer, L., Chan, C.M., McCrate, M., Chicoine, L.G., Coley, B.D., et al. (2011). Systemic gene delivery in large species for targeting spinal cord, brain, and peripheral tissues for pediatric disorders. Mol. Ther. *19*, 1971–1980.
6. Mendell, J.R., Al-Zaidy, S., Shell, R., Arnold, W.D., Rodino-Klapac, L.R., Prior, T.W., Lowes, L., Alfano, L., Berry, K., Church, K., et al. (2017). Single-dose gene-replacement therapy for spinal muscular atrophy. N. Engl. J. Med. *377*, 1713–1722.
7. Gao, G.P., Alvira, M.R., Wang, L., Calcedo, R., Johnston, J., and Wilson, J.M. (2002). Novel adeno-associated viruses from rhesus monkeys as vectors for human gene therapy. Proc. Natl. Acad. Sci. USA *99*, 11854–11859.
8. Deverman, B.E., Pravdo, P.L., Simpson, B.P., Kumar, S.R., Chan, K.Y., Banerjee, A., Wu, W.L., Yang, B., Huber, N., Pasca, S.P., and Gradinaru, V. (2016). Cre-dependent selection yields AAV variants for widespread gene transfer to the adult brain. Nat. Biotechnol. *34*, 204–209.
9. Hordeaux, J., Wang, Q., Katz, N., Buza, E.L., Bell, P., and Wilson, J.M. (2018). The neurotropic properties of AAV-PHP.B are limited to C57BL/6J mice. Mol. Ther. *26*, 664–668.
10. Holmes, C., and Stanford, W.L. (2007). Concise review: stem cell antigen-1: expression, function, and enigma. Stem Cells *25*, 1339–1347.
11. Bradfute, S.B., Graubert, T.A., and Goodell, M.A. (2005). Roles of Sca-1 in hematopoietic stem/progenitor cell function. Exp. Hematol. *33*, 836–843.
12. Morcos, M.N.F., Schoedel, K.B., Hoppe, A., Behrendt, R., Basak, O., Clevers, H.C., Roers, A., and Gerbaulet, A. (2017). SCA-1 expression level identifies quiescent hematopoietic stem and progenitor cells. Stem Cell Reports *8*, 1472–1478.
13. Park, J.W., Park, J.M., Park, D.M., Kim, D.Y., and Kim, H.K. (2016). Stem cells antigen-1 enriches for a cancer stem cell-like subpopulation in mouse gastric cancer. Stem Cells *34*, 1177–1187.
14. Zhang, Y., Chen, K., Sloan, S.A., Bennett, M.L., Scholze, A.R., O'Keeffe, S., Phatnani, H.P., Guarnieri, P., Caneda, C., Ruderisch, N., et al. (2014). An RNA-sequencing transcriptome and splicing database of glia, neurons, and vascular cells of the cerebral cortex. J. Neurosci. *34*, 11929–11947.
15. Spangrude, G.J., and Brooks, D.M. (1993). Mouse strain variability in the expression of the hematopoietic stem cell antigen Ly-6A/E by bone marrow cells. Blood *82*, 3327–3332.
16. Cray, C., Keane, R.W., Malek, T.R., and Levy, R.B. (1990). Regulation and selective expression of Ly-6A/E, a lymphocyte activation molecule, in the central nervous system. Brain Res. Mol. Brain Res. *8*, 9–15.
17. Hasin-Brumshtein, Y., Khan, A.H., Hormozdiari, F., Pan, C., Parks, B.W., Petyuk, V.A., Piehowski, P.D., Brümmer, A., Pellegrini, M., Xiao, X., et al. (2016). Hypothalamic transcriptomes of 99 mouse strains reveal trans eQTL hotspots, splicing QTLs and novel non-coding genes. eLife *5*, e15614.
18. Betley, J.N., and Sternson, S.M. (2011). Adeno-associated viral vectors for mapping, monitoring, and manipulating neural circuits. Hum. Gene Ther. *22*, 669–677.
19. Yang, Y., and Wilson, J.M. (1996). CD40 ligand-dependent T cell activation: requirement of B7-CD28 signaling through CD40. Science *273*, 1862–1864.
20. Deverman, B.E., Ravina, B.M., Bankiewicz, K.S., Paul, S.M., and Sah, D.W.Y. (2018). Gene therapy for neurological disorders: progress and prospects. Nat. Rev. Drug Discov. *17*, 641–659.
21. Penvose, A., and Westerman, K.A. (2012). Sca-1 is involved in the adhesion of myosphere cells to αVβ3 integrin. Biol. Open *1*, 839–847.
22. English, A., Kosoy, R., Pawlinski, R., and Bamezai, A. (2000). A monoclonal antibody against the 66-kDa protein expressed in mouse spleen and thymus inhibits Ly-6A.2-dependent cell-cell adhesion. J. Immunol. *165*, 3763–3771.
23. Pflugh, D.L., Maher, S.E., and Bothwell, A.L.M. (2002). Ly-6 superfamily members Ly-6A/E, Ly-6C, and Ly-6I recognize two potential ligands expressed by B lymphocytes. J. Immunol. *169*, 5130–5136.
24. Stanford, W.L., Haque, S., Alexander, R., Liu, X., Latour, A.M., Snodgrass, H.R., Koller, B.H., and Flood, P.M. (1997). Altered proliferative response by T lymphocytes of Ly-6A (Sca-1) null mice. J. Exp. Med. *186*, 705–717.
25. Ito, C.Y., Li, C.Y., Bernstein, A., Dick, J.E., and Stanford, W.L. (2003). Hematopoietic stem cell and progenitor defects in Sca-1/Ly-6A-null mice. Blood *101*, 517–523.
26. Holmes, C., Khan, T.S., Owen, C., Ciliberti, N., Grynpas, M.D., and Stanford, W.L. (2007). Longitudinal analysis of mesenchymal progenitors and bone quality in the stem cell antigen-1-null osteoporotic mouse. J. Bone Miner. Res. *22*, 1373–1386.
27. Bonyadi, M., Waldman, S.D., Liu, D., Aubin, J.E., Grynpas, M.D., and Stanford, W.L. (2003). Mesenchymal progenitor self-renewal deficiency leads to age-dependent osteoporosis in Sca-1/Ly-6A null mice. Proc. Natl. Acad. Sci. USA *100*, 5840–5845.
28. Ma, X., Robin, C., Ottersbach, K., and Dzierzak, E. (2002). The Ly-6A (Sca-1) GFP transgene is expressed in all adult mouse hematopoietic stem cells. Stem Cells *20*, 514–521.
29. Spindler, K.R., Welton, A.R., Lim, E.S., Duvvuru, S., Althaus, I.W., Imperiale, J.E., Daoud, A.I., and Chesler, E.J. (2010). The major locus for mouse adenovirus susceptibility maps to genes of the hematopoietic cell surface-expressed LY6 family. J. Immunol. *184*, 3055–3062.
30. Stier, M.T., and Spindler, K.R. (2012). Polymorphisms in Ly6 genes in Msq1 encoding susceptibility to mouse adenovirus type 1. Mamm. Genome *23*, 250–258.
31. Polishchuk, R., Di Pentima, A., and Lippincott-Schwartz, J. (2004). Delivery of raft-associated, GPI-anchored proteins to the apical surface of polarized MDCK cells by a transcytotic pathway. Nat. Cell Biol. *6*, 297–307.
32. Andreone, B.J., Chow, B.W., Tata, A., Lacoste, B., Ben-Zvi, A., Bullock, K., Deik, A.A., Ginty, D.D., Clish, C.B., and Gu, C. (2017). Blood-brain barrier permeability is regulated by lipid transport-dependent suppression of caveolae-mediated transcytosis. Neuron *94*, 581–594.e5.
33. Metzner, C., Salmons, B., Günzburg, W.H., and Dangerfield, J.A. (2008). Rafts, anchors and viruses—a role for glycosylphosphatidylinositol anchored proteins in the modification of enveloped viruses and viral vectors. Virology *382*, 125–131.
34. Coyne, C.B., and Bergelson, J.M. (2006). Virus-induced Abl and Fyn kinase signals permit coxsackievirus entry through epithelial tight junctions. Cell *124*, 119–131.
35. Merkel, S.F., Andrews, A.M., Lutton, E.M., Mu, D., Hudry, E., Hyman, B.T., Maguire, C.A., and Ramirez, S.H. (2017). Trafficking of adeno-associated virus vectors across a model of the blood-brain barrier; a comparative study of transcytosis and transduction using primary human brain endothelial cells. J. Neurochem. *140*, 216–230.
36. Di Pasquale, G., and Chiorini, J.A. (2006). AAV transcytosis through barrier epithelia and endothelium. Mol. Ther. *13*, 506–516.
37. Nonnenmacher, M., and Weber, T. (2011). Adeno-associated virus 2 infection requires endocytosis through the CLIC/GEEC pathway. Cell Host Microbe *10*, 563–576.
38. Matsuzaki, Y., Konno, A., Mochizuki, R., Shinohara, Y., Nitta, K., Okada, Y., and Hirai, H. (2018). Intravenous administration of the adeno-associated virus-PHP.B capsid fails to upregulate transduction efficiency in the marmoset brain. Neurosci. Lett. *665*, 182–188.
39. Loughner, C.L., Bruford, E.A., McAndrews, M.S., Delp, E.E., Swamynathan, S., and Swamynathan, S.K. (2016). Organization, evolution and functions of the human and mouse Ly6/uPAR family genes. Hum. Genomics *10*, 10.
40. Lock, M., Alvira, M., Vandenberghe, L.H., Samanta, A., Toelen, J., Debyser, Z., and Wilson, J.M. (2010). Rapid, simple, and versatile manufacturing of recombinant adeno-associated viral vectors at scale. Hum. Gene Ther. *21*, 1259–1271.
41. Lock, M., Alvira, M.R., Chen, S.J., and Wilson, J.M. (2014). Absolute determination of single-stranded and self-complementary adeno-associated viral vector genome titers by droplet digital PCR. Hum. Gene Ther. Methods *25*, 115–125.

42. Hwang, S., Kim, E., Lee, I., and Marcotte, E.M. (2015). Systematic comparison of variant calling pipelines using gold standard personal exome variants. Sci. Rep. *5*, 17875.

43. Poplin, R., Ruano-Rubio, V., DePristo, M.A., Fennell, T.J., Carneiro, M.O., Van der Auwera, G.A., Kling, D.E., Gauthier, L.D., Levy-Moonshine, A., Roazen, D., et al. (2017). Scaling accurate genetic variant discovery to tens of thousands of samples. bioRxiv. https://doi.org/10.1186/s40246-016-0074-2.

44. Van der Auwera, G.A., Carneiro, M.O., Hartl, C., Poplin, R., Del Angel, G., Levy-Moonshine, A., Jordan, T., Shakir, K., Roazen, D., Thibault, J., et al. (2013). From FastQ data to high confidence variant calls: the Genome Analysis Toolkit best practices pipeline. Curr. Protoc. Bioinformatics *43*, 11.10.1–11.10.33.

45. DePristo, M.A., Banks, E., Poplin, R., Garimella, K.V., Maguire, J.R., Hartl, C., Philippakis, A.A., del Angel, G., Rivas, M.A., Hanna, M., et al. (2011). A framework for variation discovery and genotyping using next-generation DNA sequencing data. Nat. Genet. *43*, 491–498.

46. McKenna, A., Hanna, M., Banks, E., Sivachenko, A., Cibulskis, K., Kernytsky, A., Garimella, K., Altshuler, D., Gabriel, S., Daly, M., and DePristo, M.A. (2010). The Genome Analysis Toolkit: a MapReduce framework for analyzing next-generation DNA sequencing data. Genome Res. *20*, 1297–1303.

47. Cingolani, P., Platts, A., Wang, L., Coon, M., Nguyen, T., Wang, L., Land, S.J., Lu, X., and Ruden, D.M. (2012). A program for annotating and predicting the effects of single nucleotide polymorphisms, SnpEff: SNPs in the genome of Drosophila melanogaster strain w1118; iso-2; iso-3. Fly (Austin) *6*, 80–92.